Geochemical Perspectives Letters

The magma ocean was a huge helium reservoir in the early Earth

O. Ozgurel, R. Caracas

Supplementary Information

The Supplementary Information includes:

- Computational Details
- Figures S-1 to S-6
- Table S-1
- Supplementary Information References

Computational Details

We performed *ab initio* molecular dynamics simulations based on density functional theory as implemented in the Vienna Ab initio Simulation Package (VASP; Kresse and Hafner, 1993; Kresse and Furthmüller, 1996). A plane wave basis set is used to represent the electron density. The core electrons are kept frozen and replaced by pseudo-potentials generated by the plane augmented wave method (PAW; Blöchl, 1994; Kresse and Joubert, 1999). We used the generalised gradient approximation (GGA) in the form of PBE exchange-correlation functional (Perdew *et al*., 1996). The simulations are spin-polarised at all conditions. The kinetic energy cut-off for the planewave basis set and the augmentation charges inside the PAW spheres were set to 550 and 850 eV, respectively. Fermi smearing was used for all calculations, setting the smearing width according to the simulation temperature.

The molecular dynamics calculations have been performed within a NVT canonical ensemble with a Nosé-Hoover thermostat (Nosé, 1984; Hoover, 1985). The cubic simulation cell is composed of two melts in contact, with starting compositions corresponding to pyrolite, *i.e.* the bulk silicate Earth (McDonough and Sun, 1995) and pure iron. Pyrolite represents the magma ocean (MO), with initial stoichiometry $NaCa_2Fe_4Mg_{30}Al_3Si_{24}O_{89}$ (153 atoms; Solomatova and Caracas, 2019), whereas the core was modelled as molten iron with 108 atoms. The two melts are arranged in contact, in slabs perpendicular to the z direction. The Brillouin zone was sampled at the Gamma point.

To calculate volatilisation, we expand the volumes of the He-bearing pyrolite melts until we reach the liquid-vapor dome. Then we build the interatomic connectivity graph at each timestep. That yields a bimodal distribution, with isolated atoms and molecules and large polymers. The former constitutes the gas phase and the latter the liquid phase. To calculate partition coefficients of He between core and MO, we put in contact

pyrolite and iron melt. Then we introduce 4 He atoms on the interface between the two slabs. Additionally, a set of simulations with 8 He atoms and different starting configurations (inside the iron slab and inside the pyrolite slab) were conducted to decrease as much as possible configurational bias. We performed the simulations covering the whole range of MO adiabats at 2000–5000 K and 3–240 GPa. Simulations at 5000 K and at pressures lower than 240 GPa were discarded as the two slabs mix. Hence the setup of the simulations with two melts in contact has two advantages over the thermodynamic integration method: the equilibration of the two melts allows for an exchange of atoms, and the conditions at which the two melts completely mix are discarded, as unphysical for computing proper partitioning coefficients. The total simulation time at each temperature and pressure is at least 20 ps with a time-step of 1–4 fs, depending on the system.

The area under the partial number density curves is directly related to the amount of atoms present within the slab and can be used to calculate their concentrations, assuming that trajectories are long enough to sample the He migration in two-melt system adequately. In our simulations the average distance travelled by the He atoms is at least the full width of the slabs, thus giving them the probabilistic time to sample the two parts of the simulation box. We calculated the concentration of He within the bulk parts of the iron and the pyrolite melts and neglecting the interface region on purpose as it does not necessarily represent equilibrium. The ratio of these concentrations gives the iron to pyrolite partition coefficient of He.

To study He vaporisation from the MO, we introduced 2 or 8 He atoms to the pyrolite melt and conducted simulations at 3000 K, 4000 K and 5000 K. We consider densities ranging from 1.1–2.0 g/cm^3. Though the He concentrations are larger than the actual values, this choice is dictated by limitations in computations, and ensures higher reliability of our results. We employed the same approach as in the previous vaporisation study (Solomatova and Caracas, 2021): early atmosphere conditions are introduced to the system as a given pressure and temperature acting on magma ocean without considering the atmospheric molecular composition. Throughout the simulation, He is able to continuously trade place between the void space as vapor molecules and the bulk of the silicate melts, as dissolved in the liquid. To distinguish between the two configurations, we perform a full speciation analysis based on the connectivity matrix between the atoms. For this, bond distances were determined from the radial distribution function. The first peak in the radial distribution function approximates the average bond length, whereas the first minimum in the radial distribution function corresponds to the radius of the first coordination sphere of atom (Fig. S-1). This value is used as a geometric cut-off length to consider two atoms bonded and were used in the volatility of He in the pyrolite melts with the speciation module of the Universal Molecular Dynamics package (Caracas *et al*., 2021). Vaporised He is defined as a component not bound to the interconnected silicate melt polymer. The proportion of species in the vapor and melt phases is calculated from an average over the entire simulation. The addition of further volatiles in the MO can enhance degassing of He, by decreasing the density of the melt, and promoting the opening of gas bubbles. On the other hand, the presence of the same other volatiles in the gas bubbles raises the gas pressure which prevents He from evaporating. Consequently, there are two possible competing effects, and they need to be thoroughly studied on a case-by-case basis. We prefer not to adventure here into a too speculative discussions, and rather wait for more experimental data or computational results.

Supplementary Figures

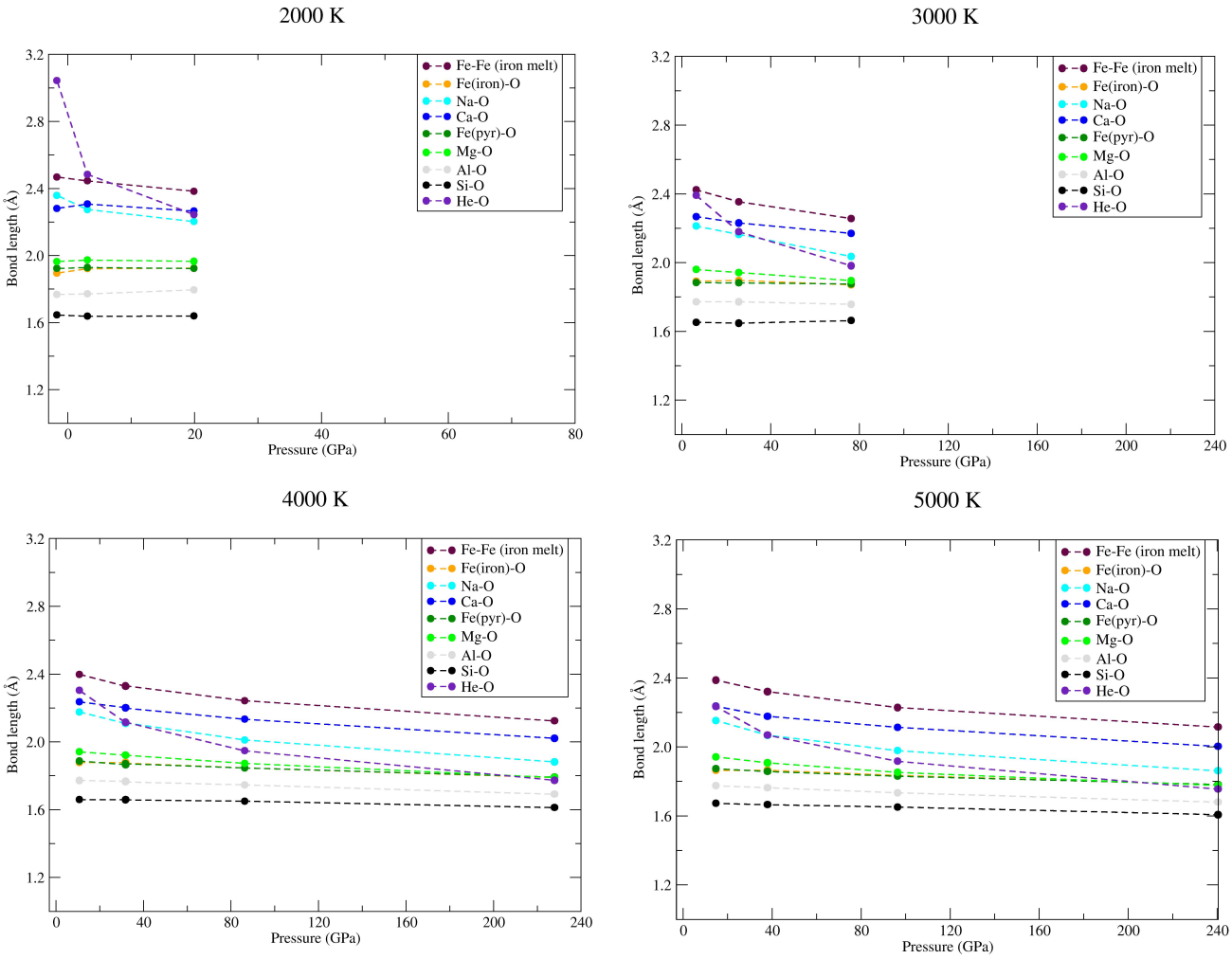

Figure S-1 Average bond lengths as a function of pressure, as approximated by the position of the first peak of the corresponding cation-oxygen radial distribution functions.

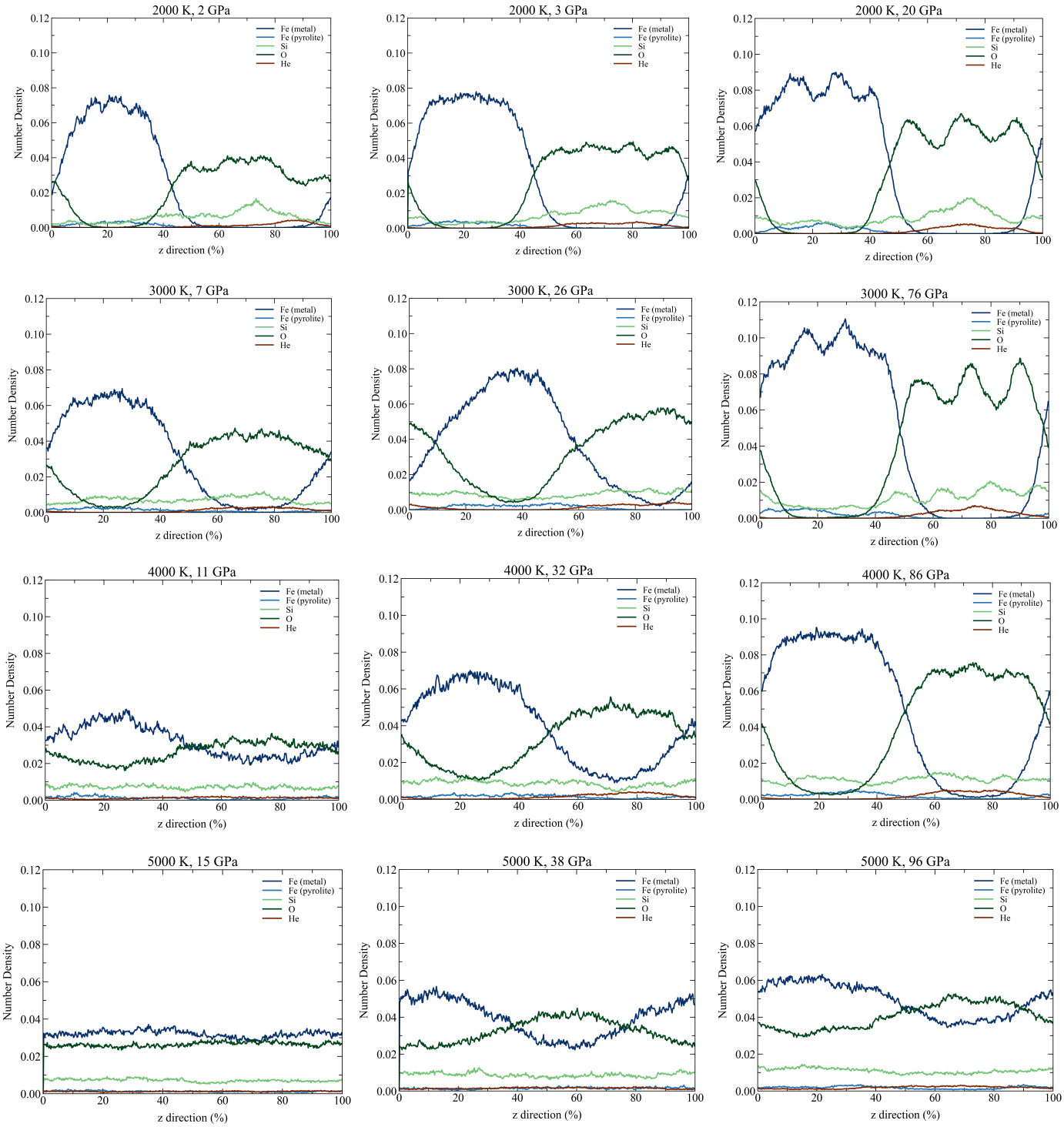

Figure S-2 Number density profiles along the *z* direction for Fe (both in metal and pyrolite), Si, O and He. 4 He atoms are introduced to the systems on the iron/pyrolite interface. From top to bottom, the temperature of the system is 2000 K, 3000 K, 4000 K and 5000 K, respectively.

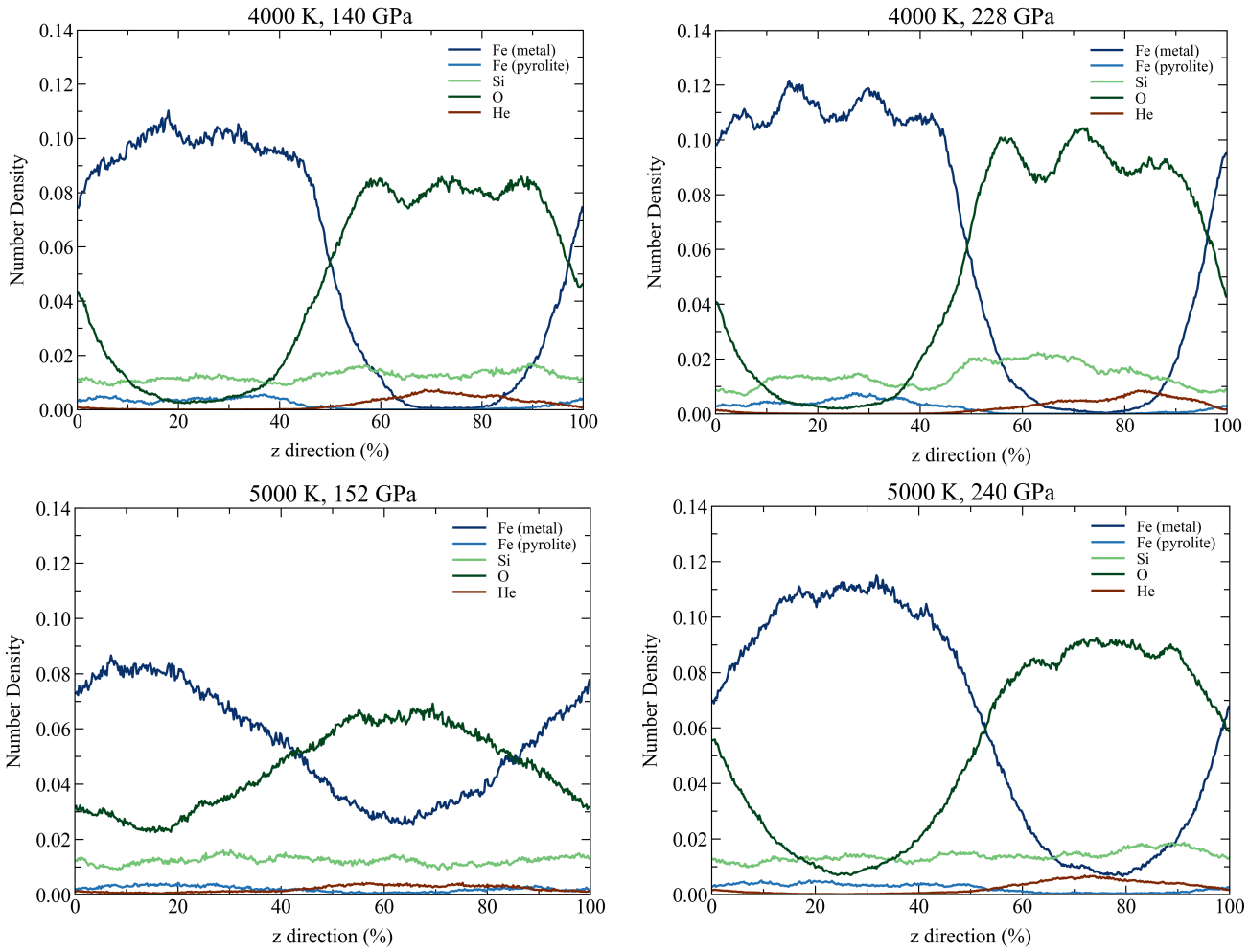

Figure S-3 Number density profiles along the *z* direction for Fe (both in metal and pyrolite), Si, O and He at high pressures (>100 GPa) and 4000 K or 5000 K. Four He atoms are introduced to the systems inside the iron slab. Four He atoms are introduced to the systems on the iron/pyrolite interface.

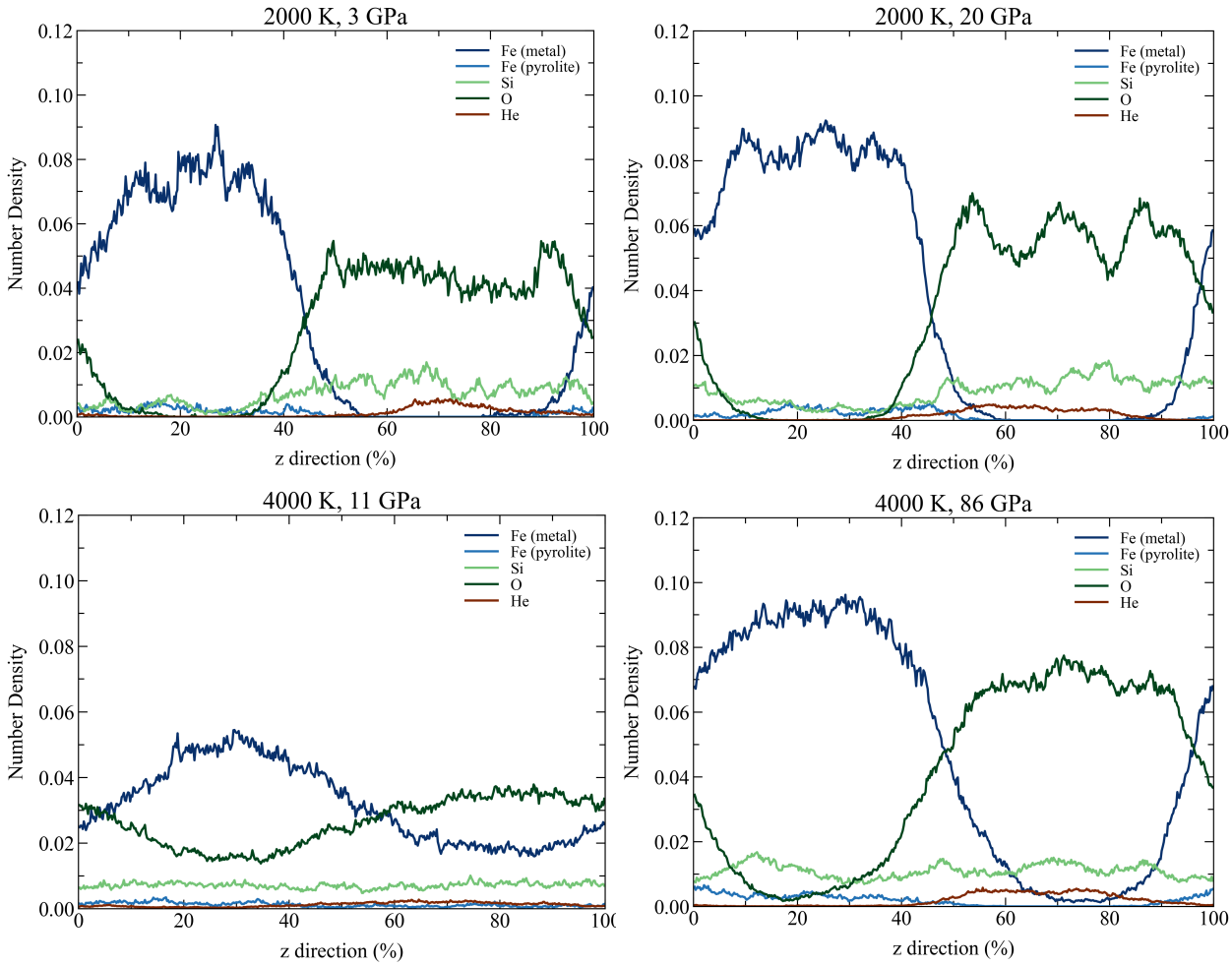

Figure S-4 Number density profiles along the *z* direction for Fe (both in metal and pyrolite), Si, O and He. Four He atoms are introduced to the systems inside the iron slab.

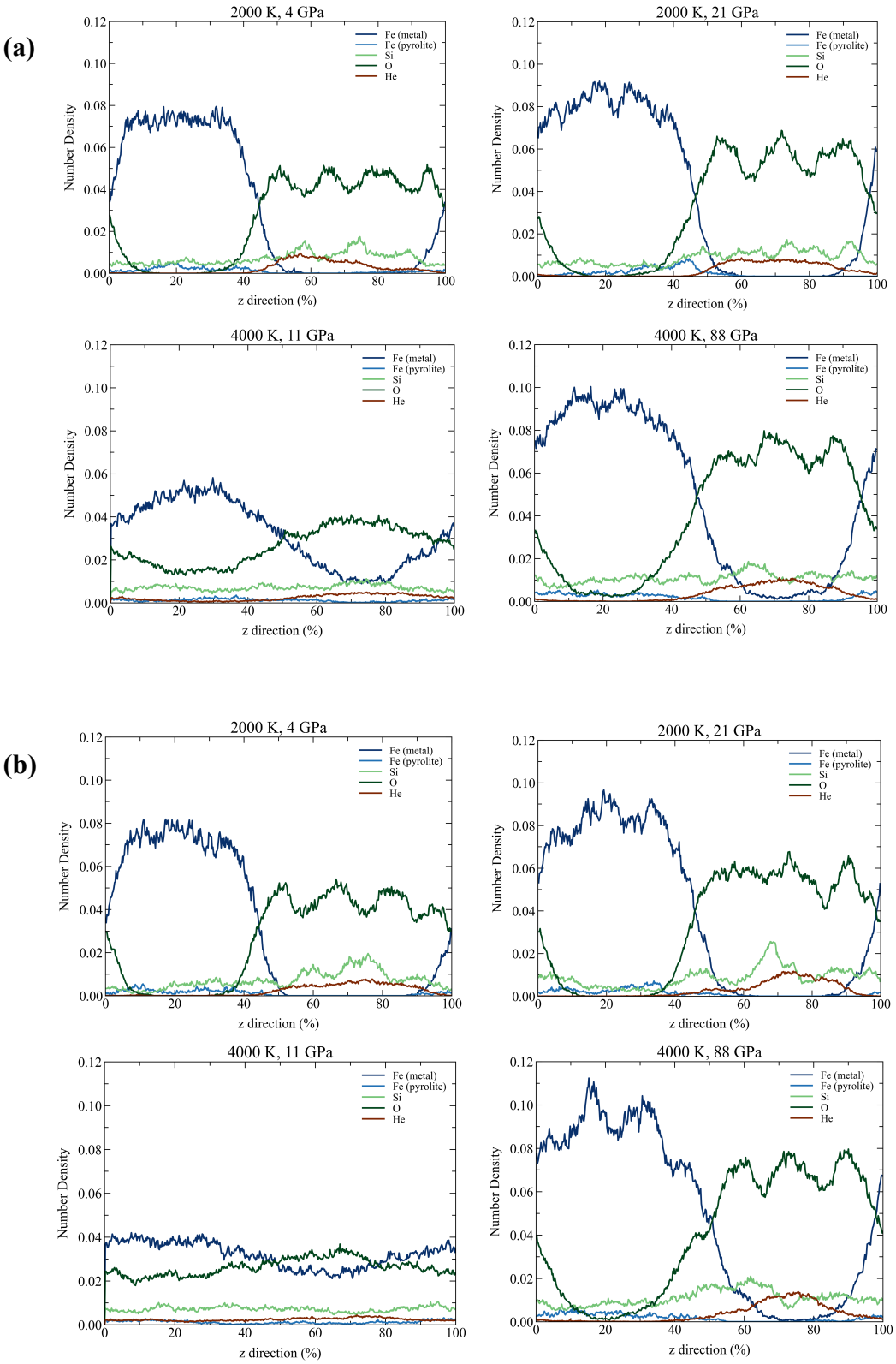

Figure S-5 Number density profiles along the *z* direction for Fe (both in metal and pyrolite), Si, O and He. Eight He atoms are introduced in the simulations inside **(a)** the pyrolite slab and **(b)** the iron slab.

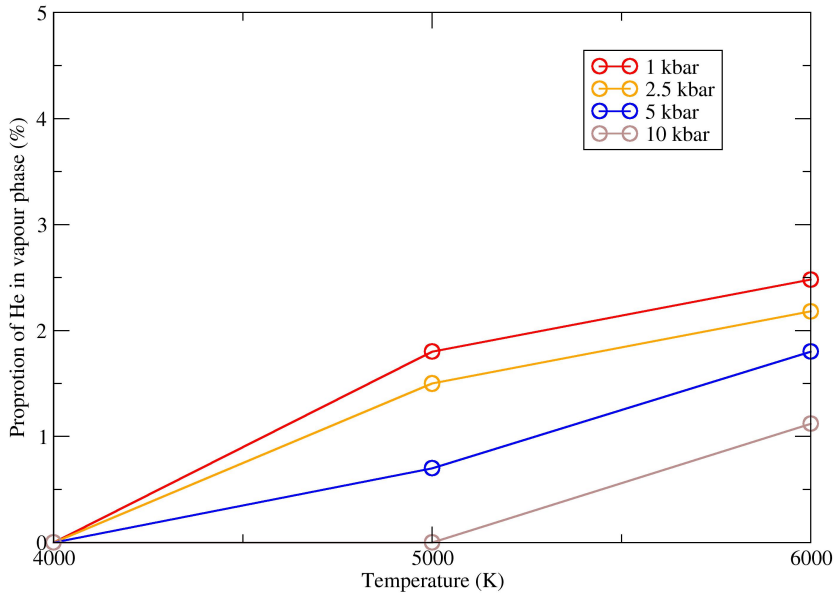

Figure S-6 Proportion of vaporised He as a function of temperature along isobars of 1 to 10 kbar.

Supplementary Table

Table S-1 Zero-pressure density (ρ_0), zero-pressure bulk modulus (K_0) and the first derivative of the bulk modulus (K') at 4000–6000 K, obtained from fitting a third-order Birch Murnaghan (BM) equation of state to the pressure-density data.

T (K)	ρ_0 (g/cm^3)	K_0 (GPa)	K'
4000	2.04	11.1	5.5
5000	1.79	6.6	5.9
6000	1.64	6.1	5.4

Supplementary Information References

Blöchl, P.E. (1994) Projector augmented-wave method. *Physical Review B* 50, 17953. https://doi.org/10.1103/PhysRevB.50.17953

Caracas, R., Kobsch, A., Solomatova, N.V., Li, Z., Soubiran, F., Hernandez, J.-A. (2021) Analyzing Melts and Fluids from Ab Initio Molecular Dynamics Simulations with the UMD Package. *Journal of Visualized Experiments* 175, e61534. https://doi.org/10.3791/61534

Hoover, W.G. (1985) Canonical dynamics: Equilibrium phase-space distributions. *Physical Review A* 31, 1695. https://doi.org/10.1103/PhysRevA.31.1695

Kresse, G., Hafner, J. (1993) *Ab initio* molecular dynamics for liquid metals. *Physical Review B* 47, 558. https://doi.org/10.1103/PhysRevB.47.558

Kresse, G., Furthmüller, J. (1996) Efficient iterative schemes for *ab initio* total-energy calculations using a plane-wave basis set. *Physical Review B* 54, 11169. https://doi.org/10.1103/PhysRevB.54.11169

Kresse, G., Joubert, D. (1999) From ultrasoft pseudopotentials to the projector augmented-wave method. *Physical Review B* 59, 1758. https://doi.org/10.1103/PhysRevB.59.1758

McDonough, W.F., Sun, S.-s. (1995) The composition of the Earth. *Chemical Geology* 120, 223–253. https://doi.org/10.1016/0009-2541(94)00140-4

Nosé, S. (1984) A unified formulation of the constant temperature molecular dynamics methods. *The Journal of Chemical Physics* 81, 511–519. https://doi.org/10.1063/1.447334

Perdew, J.P., Burke, K., Wang, Y. (1996) Generalized gradient approximation for the exchange-correlation hole of a many-electron system. *Physical Review B* 54, 16533. https://doi.org/10.1103/PhysRevB.54.16533

Solomatova, N.V., Caracas, R. (2019) Pressure-Induced Coordination Changes in a Pyrolitic Silicate Melt From Ab Initio Molecular Dynamics Simulations. *Journal of Geophysical Research: Solid Earth* 124, 11232–11250. https://doi.org/10.1029/2019JB018238

Solomatova, N.V., Caracas, R. (2021) Genesis of a CO_2-rich and H_2O-depleted atmosphere from Earth's early global magma ocean. *Science Advances* 7, eabj0406. https://doi.org/10.1126/sciadv.abj0406